Received: Added at production | Revised: Added at production | Accepted: Added at production

DOI: xxx/xxxx

ARTICLE TYPE

Fractional-Order Integral Terminal Sliding-Mode Control for Perturbed Nonlinear Systems With Application to Quadrotors

M. Labbadi*[1] | M. Defoort[1] | G. P. Incremona[2] | M. Djemai[1]

[1] Univ. Polytechnique Hauts-de-France, INSA Hauts-de-France, LAMIH, CNRS, UMR 8201, F-59313 Valenciennes, France

[2] Dipartimento di Elettronica, Informazione e Bioingegneria, Politecnico di Milano, Piazza Leonardo da Vinci 32, 20133, Milano, Italy

Correspondence
*Corresponding author Moussa Labbadi, Corresponding address. Email: moussa.labbadi@uphf.fr

Present Address
Univ. Polytechnique Hauts-de-France, INSA Hauts-de-France, LAMIH, CNRS, UMR 8201, F-59313 Valenciennes, France

Abstract

In this paper, a novel fractional-order recursive integral terminal sliding mode (FORITSM) control is proposed for nonlinear systems in the presence of external disturbances with unknown bounds. The proposed control approach provides an easy-to implement solution capable of zeroing the sliding variable in a finite-time (FnT) by adding a fractional-order command filter. Moreover, the reaching phase is eliminated, and FnT convergence of the system states is proved. The proposed technique has also a chattering alleviation property, which is beneficial for practical cases, as the control of quadrotor UAVs presented in the paper. Finally, a simulation case study on a quadrotor system is illustrated to show the effectiveness of the proposed FORITSM control, also with respect to classical methods.

KEYWORDS:
Chattering alleviation, FnT, fractional-order recursive integral terminal sliding mode, full-order sliding mode, reaching phase, uncertain systems.

1 | INTRODUCTION

Sliding mode control (SMC) is a powerful easy-to-implement control technique with remarkable robustness properties in case of systems affected by disturbances and unavoidable modelling uncertainties [1,2,4]. The goal of SMC in its classical version is to compel the behavior of a dynamical system according to a manifold, i.e., the so-called “sliding surface”, specified by a function known as “sliding variable”, via a discontinuous controller depending on the sliding variable itself.

Once the sliding variable is zeroed, that is a "sliding mode” is enabled, it can be proved that the controlled system is insensitive to the uncertainty terms fulfilling a matched condition. Moreover, the key feature of the SMC method is the capability to enable a finite-time convergence of the sliding variable towards the sliding surface, thus implying an equivalent reduced order dynamics, for which asymptotic stability of the system trajectories is guaranteed. However, more recently, advanced techniques extended the original SMC concept by enhancing the robustness properties of the controlled system through the introduction of integral methods [3], or by introducing state constraints [5], or enabling also a FnT convergence of the system trajectories by using terminal sliding modes [7].

1.1 | Background and motivations

In this paper, we consider the family of the terminal sliding mode (TSM) controllers. As previously mentioned, this type of control law guarantees that, if the sliding mode exists, this allows to regulate the system trajectories in FnT. Nevertheless, the main drawback of TSM is the occurrence of singularity in the control signal, which could cause system instability [8]. Specifically,

in [8] such technical concerns and future challenges have been discussed in the perspective of a broader scope of technological advances such as cyber-physical systems, artificial intelligence, and network systems, providing a summary of the state of the art in TSM control theory and applications.

To avoid the singularity problem, nonsingular TSM (NTSM) controllers have been developed in recent years, see [9] or [11], where a finite-time stabilizing method based on the SMC strategy was devised to handle this issue. Aside from singularity, TSM and NTSM control approaches suffer the generation of chattering phenomenon due to the discontinuity of the control function, resulting in high-frequency oscillations of the system states, which can damage mechanical components and lead to input saturation when employed in nonlinear systems [10,12].

Several methods have been introduced in the literature for reducing chattering, including the boundary layer method [13], the high-order sliding-mode method [14,15], and the disturbance estimation method [16]. In the case of boundary layer approach, the saturation function or sigmoid function are adopted. This choice gives rise to a "pseudo-sliding mode", since only a vicinity of the sliding surface is reached, thus possibly causing the loss of robustness of the system in front of disturbances. As for high-order sliding-mode (HOSM) control approaches, they allow to confine the discontinuity to the derivative of the control input while the signal actually fed into the plant is continuous. The disturbance estimation method is instead based on the design of an asymptotic disturbance observer to compensate for the disturbance, thus allowing a smoother control signal [16]. Among many other approaches, recently, the combination of internal model principle and adaptive sliding mode control, as proposed in [6], allows a reduction of the control authority to dominate the uncertainties with a consequent chattering reduction.

Another drawback of the presented SMCs is the length of the reaching phase (RP) and the sensitivity of the controlled system to perturbation during such an interval. Many works have been developed to address these problems, see e.g., [18,19,20]. As for integral HOSM controllers, these are instead discussed in [21] for uncertain nonlinear systems to remove the RP, although the input singularity generated by the sliding function is not studied in depth.

Moreover, to avoid the problem of “complexity explosion”, command filtering can be used. For example, in [22] a command filtered and adaptive control is proposed, while a command filter-using fractional-order dynamics in the design of sliding mode manifold is presented in [23,24]. A command filtered based-backstepping technique is suggested in [27], and a FnT adaptive control is developed in [28]. Also command-filter-based adaptive fuzzy FnT control approaches have been proposed as those in [25,26,28].

1.2 | Contributions

This main contribution of this paper is the design of a novel robust fractional-order FnT control for perturbed nonlinear systems, capable of alleviating chattering phenomena and without singularity. Differently from the existing literature, where a reduction of the reaching phase is adopted [9,10], here, making reference to [12], a command-filter based fractional-order (FO) recursive nonsingular terminal SMC is presented for the first time, to the best of the authors' knowledge. By employing the fractional-order of the input in the controller, chattering reduction of the input is achieved. In the presence of external perturbations, the presented Lyapunov-based analysis shows that the system trajectories under the proposed control action can converge to the origin in FnT. Finally, to assess the proposed strategy in a practical example, a quadrotor dynamics is considered and several simulations in different scenarios are provided. Overall, more in detail, the contributions of this paper are summarized as follows:

(i) To improve the convergence of the standard integer-order FnT command filter and avoid an “explosion of complexity”, a fractional-order finite-time command filter based on recursive nonsingular terminal SMC is introduced for full-order nonlinear system.

(ii) The fractional-order control input is produced in a nonsingular fractional-order integral form rather than a standard signum function, which is useful for reducing control input chattering. Furthermore, when compared to integral HOSM controllers [17], the FORITSM control only has two layers of sliding manifolds, which makes it easier to build for high-order systems.

(iii) Based on this fractional-order recursive structure of the control law, the RP is eliminated, thus enhancing the robustness of the controlled system.

(iv) The proposed control method has been applied for quadrotor dynamics and compared with the work developed in [12].

1.3 | Outline of the paper

The paper is organized as follows. After some preliminaries and the problem statement in Section 2, the main results on the proposed fractional-order finite-time control are given in Section 3. The application to the tracking control problem for a quadrotor dynamics is addressed in Section 4, while simulations are illsutrated in Section 5. Finally, some conclusions are gathered in Section 6.

Notation

The main notation and opertators used in the paper are hereafter recalled. Let $x \in \mathbb{R}$, then the absolute value of x, denoted by $|x|$, is defined as $|x| = x$ if $x \geq 0$, and $|x| = -x$ if $x < 0$. The function $\text{sign}(x)$ is defined as $\text{sign}(x) = 1$ for $x > 0$, $\text{sign}(x) = -1$ for $x < 0$, and $\text{sign}(x) = 0$ for $x = 0$. For $\gamma \geq 0$, one has that $\text{sig}^{\gamma}(x) = |x|^{\gamma}\,\text{sign}(x)$, so that $\text{sig}^{0}(x) = \text{sign}(x)$.

2 | PRELIMINARIES AND PROBLEM FORMULATION

In this section, some preliminaries on fractional calculus and Mittag-leffler functions are recalled. Then, the considered control problem is formulated.

2.1 | Preliminaries on fractional calculus

Let us recall some definitions concerning fractional order derivatives. For any real number $\alpha > 0$ (namely, the derivative order), the Riemann-Liouville fractional derivative for a function $\Psi : [a, \infty) \to \mathbb{R}$ is given by[29,30]

$$ {}^{RL}_{a}D^{\alpha}_{t}\Psi(t) = \frac{1}{\Gamma(\Upsilon-\alpha)}\frac{d^{\Upsilon}}{dt^{\Upsilon}}\int_{a}^{t}\frac{\Psi(\tau)}{(t-\tau)^{\alpha-\Upsilon+1}}d\tau, \tag{1} $$

where $\Upsilon \in \mathbb{N}^{*}$ is such that $(\Upsilon - 1) < \alpha < \Upsilon$ and $\Gamma(\cdot)$ is the Gamma function expressed as

$$ \Gamma(K) = \int_{0}^{\infty} \mathrm{e}^{-t}t^{K-1}dt. \tag{2} $$

Furthermore, for any real number $\alpha > 0$, the Caputo fractional derivative (CFD) for a function $\Psi : [a, \infty) \to \mathbb{R}$ is given by[30,31]

$$ {}^{C}_{a}D^{\alpha}_{t}\Psi(t) = \frac{1}{\Gamma(\alpha-\Upsilon)}\int_{a}^{t}\frac{\Psi^{(\Upsilon)}(\tau)}{(t-\tau)^{\alpha-\Upsilon+1}}d\tau. \tag{3} $$

Some important properties are recalled hereafter.

Property 1. For any real numbers $\alpha \geq \lambda \geq 0$, the CFD for a function $\Psi : [t_0, \infty) \to \mathbb{R}$ satisfies

$$ {}^{C}_{t_0}D^{\alpha}_{t}({}^{C}_{t_0}D^{-\lambda}_{t}\Psi(t)) = {}^{C}_{t0}D^{\alpha-\lambda}_{t}\Psi(t). \tag{4} $$

Property 2. Let $0 < \alpha < 1$ and $\Psi : [t_0, \infty) \to \mathbb{R}$, then the following equality holds:

$$ {}^{C}_{t_0}D^{1-\alpha}_{t}({}^{C}_{t_0}D^{\alpha}_{t}\Psi(t)) = {}^{C}_{t_0}D^{\alpha}_{t}({}^{C}_{t_0}D^{1-\alpha}_{t}\Psi(t)) = \dot{\Psi}(t). \tag{5} $$

In the following, the operator ${}^{C}_{t_0}D^{\alpha}_{t}$ will be replaced by D^{α} throughout this paper.

2.2 | Mittag-Leffler type functions

The Mittag-Leffler function[29,30] can be defined as:

$$ E_{\xi}(X) = \sum_{\rho=0}^{\infty}\frac{X^{\rho}}{\Gamma(\rho\xi+1)}, \tag{6} $$

with ρ being a strictly positive constant. When two arguments are taken into account, the Mittag-Leffler function becomes

$$E_{\xi_1,\xi_2}(X) = \sum_{\rho=0}^{\infty} \frac{X^{\rho}}{\Gamma(\rho\xi_1 + \xi_2)}, \tag{7}$$

with $\xi_1, \xi_2 > 0$. Hence, one has $E_{\xi}(X) = E_{\xi_1,1}(X)$ and $E_{1,1}(X) = e^X$.

2.3 | Problem statement

Consider the following nonlinear system

$$\begin{cases} \dot{\mathcal{Z}}_1 &= \mathcal{Z}_2 \\ \dot{\mathcal{Z}}_2 &= \mathcal{Z}_3 \\ &\vdots \\ \dot{\mathcal{Z}}_{n-1} &= \mathcal{Z}_n \\ \dot{\mathcal{Z}}_n &= \mathcal{F}(\mathcal{Z}) + \mathcal{G}(\mathcal{Z})\mathcal{U} + \mathcal{D}(\mathcal{Z}, t), \end{cases} \tag{8}$$

where the state vector is $\mathcal{Z} = [\mathcal{Z}_1, \mathcal{Z}_2, ..., \mathcal{Z}_n]^T \in \mathbb{R}^n$ and the control input is $\mathcal{U} \in \mathbb{R}$. Furthermore, $\mathcal{F}(\mathcal{Z})$ and $\mathcal{G}(\mathcal{Z}) \neq 0$ are two known nonlinear functions, while $\mathcal{D}(\mathcal{Z}, t)$ represents uncertainties and external disturbances.

Assumption 1. It is assumed that $\mathcal{D}(\mathcal{Z}, t) < \Upsilon_T$ and $\dot{\mathcal{D}}(\mathcal{Z}, t) < \Upsilon_d$ where $\Upsilon_T >$ and $\Upsilon_d >$.

The control objective is to design a robust controller which guarantees FnT stability of the origin of the closed-loop system (8) without knowing the upper bound of the disturbances. The following lemmas will be useful to derive the main results.

Lemma 1 ([12])**.** Consider the sliding variable

$$\mathcal{S} = \dot{\mathcal{Z}}_n + \kappa_n \text{sign}\left(\mathcal{Z}_n\right) \left|\mathcal{Z}_n\right|^{\mu_n} + ... + \kappa_1 \text{sign}\left(\mathcal{Z}_1\right) \left|\mathcal{Z}_1\right|^{\mu_1}, \tag{9}$$

where μ_j and κ_j $(j = 1, 2, ..., n)$ are positive constants such that the polynomial $p^n + \kappa_n p^{n-1} + ... + \kappa_2 p + \kappa_1$ is Hurwitz and

$$\begin{cases} \mu_1 &= \mu, \\ \mu_{j-1} &= \frac{\mu_j \mu_{j+1}}{2\mu_{j+1} - \mu_j}, \ j = 1, 2, ..., n, \quad \forall n \geq 2 \end{cases} \tag{10}$$

with $\mu_{n+1} = 1$, $\mu_n = \mu$, $\mu \in (1 - \epsilon, 1)$ and $\epsilon \in (0, 1)$. Once the sliding mode is established (i.e., $\mathcal{S} = 0$), the system state converges to zero in FnT.

Theorem 1. (Refer to Reference [12]) If the sliding-mode surface s is selected as (9) and the control is built as follows (11), the nonlinear system (**??**) will approach $\mathcal{S} = 0$ in finite time and then converge to zero along $\mathcal{S} = 0$ in FnT.

$$\mathcal{U} = \frac{1}{\mathcal{G}(\mathcal{Z})} \left(\mathcal{U}_0 + \mathcal{U}_1\right), \tag{11}$$

$$\mathcal{U}_0 = -\mathcal{F}(\mathcal{Z}) - \kappa_n sign\left(\mathcal{Z}_n\right) \left|\mathcal{Z}_n\right|^{\mu_n} - ... - \kappa_1 sign\left(\mathcal{Z}_1\right) \left|\mathcal{Z}_1\right|^{\mu_1} \tag{12}$$

$$\begin{aligned} \dot{\mathcal{U}}_1 + \mathcal{T}\mathcal{U}_1 &= \varsigma, \\ \varsigma &= -\left(\Upsilon_d + \Upsilon_T + \varsigma_0\right) sign(\sigma) \end{aligned} \tag{13}$$

where Υ_d, Υ_T, ς are positive parameters.

Lemma 2 ([17])**.** Consider the first-order nonlinear differential equation

$$\dot{\Upsilon} + \Lambda \text{sig}\left(\Upsilon\right)^{\beta} = 0, \tag{14}$$

with $\Lambda > 0$, $0 < \beta < 1$. Then, Υ converges to zero in a finite-time given by

$$t_f = \frac{|\Upsilon(0)|^{1-\beta}}{\Lambda(1-\beta)}. \tag{15}$$

3 | THE PROPOSED FORITSM CONTROL LAW

To design the proposed robust controller, let us consider the following fractional-order integral terminal sliding variable, i.e.,

$$\sigma = \mathcal{S} + \Lambda D^{\beta-1}\mathcal{S}_I \tag{16}$$

with $\Lambda > 0$, $0 < \beta < 1$. The sliding variable $\mathcal{S}$ is given in (9) and $\mathcal{S}_I$ can be designed as:

$$D^{\beta}\mathcal{S}_I = \text{sign}(\mathcal{S})|\mathcal{S}|^{\alpha}, \tag{17}$$

with initial value

$$\mathcal{S}_I(0) = -\frac{1}{\Lambda}D^{1-\beta}\mathcal{S}(0). \tag{18}$$

From Eqs. (16)-(18) , one can easily see that $\sigma(0) = 0$. Hence, the reaching phase to the sliding surface $\sigma = 0$ is removed.

Remark 1. The proposed recursive form terminal sliding variable (16) combines two sliding variables (i.e., (9) and (17)). If an appropriate control input is designed such that the sliding mode is established (i.e., $\sigma = 0$), the system trajectories will be constrained to the sliding surface $\sigma = 0$, and then to the origin in FnT. Because of the integral initial condition in (18), the RP is cancelled in comparison to conventional TSM control. Moreover, compared to integral HOSM control, only two layers of sliding manifolds are adopted in the integral TSM, which is simpler for practical implementations. In addition, the proposed sliding manifold offers extract degree to increase the performance tracking of the full nonlinear system.

Compute now the time derivative of σ, i.e.,

$$\begin{aligned}\dot{\sigma} =& \dot{\mathcal{S}} + \Lambda D^{\beta}\mathcal{S}_{I\beta} \\ =& \ddot{\mathcal{Z}}_n + \kappa_n\mu_n\left|\mathcal{Z}_n\right|^{\mu_n-1}\dot{\mathcal{Z}}_n + ... + \kappa_n\mu_n\left|\mathcal{Z}_1\right|^{\mu_1-1}\dot{\mathcal{Z}}_1 + \Lambda D^{\beta}\mathcal{S}_{I\beta}.\end{aligned} \tag{19}$$

Theorem 2. Given the nonlinear system (8), consider the sliding variable (16) and the following controller

$$\mathcal{U} = \mathcal{G}(\mathcal{Z})^{-1}\left(\mathcal{U}_0 + \mathcal{U}_1\right) \tag{20}$$

$$\mathcal{U}_0 = -\mathcal{F}(\mathcal{Z}) - \kappa_n\text{sign}\left(\mathcal{Z}_n\right)\left|\mathcal{Z}_n\right|^{\mu_n} - ... - \kappa_1\text{sign}\left(\mathcal{Z}_1\right)\left|\mathcal{Z}_1\right|^{\mu_1} - \Lambda D^{\beta}\mathcal{S}_I \tag{21}$$

$$\begin{aligned}D^{\lambda}\mathcal{U}_1 + \mathcal{T}\mathcal{U}_1 = \zeta_I,& \\ \zeta_I = -\left(\Upsilon_d + \Upsilon_T + \varsigma_0\right)D^{\lambda-1}\text{sign}(\sigma) - K_f D^{\lambda-1}\sigma,&\end{aligned} \tag{22}$$

with $\kappa_j > 0$, $\Upsilon_d, \Upsilon_T, \varsigma_0$ being positive constants, λ being a fractional operator, and the two constants Υ_d and Υ_T chosen such that $\Upsilon_T > \mathcal{T}\delta$. Then, the trajectories of (8), constrained to $\sigma = 0$, will converge to zero in a FnT.

Proof. Making reference to system (8), the sliding variable (16) can be expressed as

$$\begin{aligned}\sigma =& \dot{\mathcal{Z}}_n + \kappa_n\text{sign}\left(\mathcal{Z}_n\right)\left|\mathcal{Z}_n\right|^{\mu_n} + ... + \kappa_1\text{sign}\left(\mathcal{Z}_1\right)\left|\mathcal{Z}_1\right|^{\mu_1} + \Lambda D^{\beta-1}\mathcal{S}_I \\ =& \mathcal{F}(\mathcal{Z}) + \mathcal{G}(\mathcal{Z})\mathcal{U} + \mathcal{D}(\mathcal{Z},t) + \kappa_n\text{sign}\left(\mathcal{Z}_n\right)\left|\mathcal{Z}_n\right|^{\mu_n} + ... + \kappa_1\text{sign}\left(\mathcal{Z}_1\right)\left|\mathcal{Z}_1\right|^{\mu_1} + \Lambda D^{\beta-1}\mathcal{S}_I.\end{aligned} \tag{23}$$

Replacing the control (20) into equation (23) yields

$$\begin{aligned}\sigma =& \mathcal{F}(\mathcal{Z}) + \mathcal{U}_0 + \mathcal{U}_1 + \mathcal{D}(\mathcal{Z}) + \kappa_n\text{sign}\left(\mathcal{Z}_n\right)\left|\mathcal{Z}_n\right|^{\mu_n} + ... + \kappa_1\text{sign}\left(\mathcal{Z}_1\right)\left|\mathcal{Z}_1\right|^{\mu_1} + \Lambda D^{\beta-1}\mathcal{S}_I \\ =& \mathcal{U}_1 + \mathcal{D}(\mathcal{Z}).\end{aligned} \tag{24}$$

The FO switching law can be written as

$$D^{\lambda}\mathcal{U}_1 + \mathcal{T}\mathcal{U}_1 = -\left(\Upsilon_d + \Upsilon_T + \varsigma_0\right)D^{\lambda-1}\text{sign}(\sigma) - K_f D^{\lambda-1}\sigma \tag{25}$$

$$= -D^{\lambda-1}\left[\left(\Upsilon_d + \Upsilon_T + \varsigma_0\right)\text{sign}(\sigma) - K_f\sigma\right]. \tag{26}$$

After simple calculation, one has

$$\dot{\mathcal{U}}_1 + \mathcal{T}D^{1-\lambda}\mathcal{U}_1 = -\underbrace{\left(\Upsilon_d + \Upsilon_T + \varsigma_0\right)\text{sign}(\sigma) - K_f\sigma}_{\zeta_I}. \tag{27}$$

Since the Laplace transform of Eq. (27) is

$$s\mathcal{U}_1(s) - \mathcal{U}_1(0) + \mathcal{T}s^{1-\lambda}\mathcal{U}_1(s) - \mathcal{T}s^{-\lambda}\mathcal{U}_1(0) = \zeta_I(s), \tag{28}$$

with non negative constant $\mathcal{U}_1(0) = \mathcal{U}_1(0, \sigma(0))$, then Eq. (28) can be defined as

$$\mathcal{U}_1(s) = \frac{\zeta_I(s)s^{-1} + \mathcal{U}_1(0)s^{-1} + s^{-1-\lambda}\mathcal{U}_1(0)}{1 + \mathcal{T}s^{-\lambda}} \tag{29}$$

The unique solution of (29) arises from the uniqueness and existence theorem of fractional equations[29] and the properties of inverse Laplace transform since $\mathcal{U}_1(t, \sigma)$ is locally Lipschitz with respect to σ. The solution of (25) is given by:

$$\mathcal{U}_1(t) = \mathcal{U}_1(0)t^{-\lambda}E_{-\lambda,-\lambda+1}\left(-\mathcal{T}t^{-\lambda}\right) + \mathcal{U}_1(0)E_{-\lambda}\left(-\mathcal{T}t^{-\lambda}\right) + \int_0^t \left(t-\tau\right)^{-\lambda} E_{-\lambda,-\lambda+1}\left(-\mathcal{T}\left(t-\tau\right)^{-\lambda}\right)\zeta_I(\tau)d\tau, \tag{30}$$

where $E_{-\lambda}\left(-\mathcal{T}t^{\lambda}\right)$ and $E_{-\lambda,-\lambda+1}\left(-\mathcal{T}t^{\lambda}\right)$ are Mittag-Leffler functions.

Using the condition $\Upsilon_T > \mathcal{T}\delta$ and from (24) and (30), under the condition $\mathcal{U}_1(0) = 0$, one obtains $\Upsilon_T \geq \mathcal{T}$, $\Upsilon_d \geq \mathcal{T}$, and $\left|\mathcal{U}_1\right|_{\max} \geq \mathcal{T}\left|\mathcal{U}_1(t)\right|$, which in turn implies $\mathcal{T}\left|\mathcal{U}_1(t)\right| \leq \Upsilon_T$. The fractional derivative of the terminal sliding manifold (24) is

$$\begin{aligned} D^{\lambda}\sigma &= D^{\lambda}\mathcal{D}(\mathcal{Z}) + D^{\lambda}\mathcal{U}_1 && (31)\\ &= D^{\lambda}\mathcal{D}(\mathcal{Z}) + D^{\lambda}\mathcal{U}_1 + \mathcal{T}\mathcal{U}_1 - \mathcal{T}\mathcal{U}_1 && (32)\\ &= D^{\lambda}\mathcal{D}(\mathcal{Z}) + \zeta_I - \mathcal{T}\mathcal{U}_1 && (33)\\ &= D^{\lambda}\mathcal{D}(\mathcal{Z}) - D^{\lambda-1}\left[\left(\Upsilon_d + \Upsilon_T + \varsigma_0\right)\mathrm{sign}(\sigma) - K_f\sigma\right] - \mathcal{T}\mathcal{U}_1. && (34)\end{aligned}$$

Consider now the Lyapunov function and its time-derivative as $\mathcal{V} = \frac{1}{2}\sigma^2$ and $\dot{\mathcal{V}} = \sigma\dot{\sigma} = \sigma D^{1-\lambda}(D^{\lambda}\sigma)$. One gets

$$\begin{aligned} \dot{\mathcal{V}} &= \sigma D^{1-\lambda}\{D^{\lambda}\mathcal{D}(\mathcal{Z}) - D^{\lambda-1}\left[\left(\Upsilon_d + \Upsilon_T + \varsigma_0\right)sign(\sigma) - K_f\sigma\right] - \mathcal{T}\mathcal{U}_1\} && (35)\\ &= \sigma\{\dot{\mathcal{D}}(\mathcal{Z}) - \left[\left(\Upsilon_d + \Upsilon_T + \varsigma_0\right)sign(\sigma) - K_f\sigma\right] - \mathcal{T}D^{1-\lambda}\mathcal{U}_1\} && (36)\\ &= \dot{\mathcal{D}}(\mathcal{Z})\sigma - \left(\Upsilon_d + \Upsilon_T + \varsigma_0\right)|\sigma| - K_f\sigma^2 - \mathcal{T}D^{1-\lambda}\mathcal{U}_1\sigma && (37)\\ &\leq \left|\dot{\mathcal{D}}(\mathcal{Z})\right||\sigma| - \Upsilon_d|\sigma| + \left[-\mathcal{T}D^{1-\lambda}\mathcal{U}_1\sigma - \Upsilon_T|\sigma|\right] - \varsigma_0|\sigma| - K_f\sigma^2 && (38)\end{aligned}$$

According to the Assumption (1) and exploiting (35), one gets

$$\dot{\mathcal{V}} = \sigma\dot{\sigma} \leq -\varsigma_0|\sigma| - K_f\sigma^2. \tag{39}$$

To demonstrate the finite-time stability, (39) can be rewritten as

$$\dot{\mathcal{V}} \leqslant -2K_f\mathcal{V} - \sqrt{2}\varsigma_0\mathcal{V}^{\frac{1}{2}}. \tag{40}$$

Dividing (40) by $\mathcal{V}^{\frac{1}{2}}$, one obtains

$$dt \leqslant -\frac{\mathcal{V}^{-\frac{1}{2}}}{2K_f\mathcal{V}^{\frac{1}{2}} + \sqrt{2}\varsigma_0}d\mathcal{V}. \tag{41}$$

By integrating (41) from t_0 to t_c and after a simple calculation, it yields

$$\begin{aligned} t_c - t_0 &\leqslant -\int_{\mathcal{V}(t_{x0})}^{0} \frac{\mathcal{V}^{-\frac{1}{2}}}{2K_f\mathcal{V}^{\frac{1}{2}} + \sqrt{2}\varsigma_0}d\mathcal{V} && (42)\\ &= \frac{1}{K_f}ln\frac{2K_f\mathcal{V}^{\frac{1}{2}}(t_{x0}) + \sqrt{2}\varsigma_0}{\sqrt{2}\varsigma_0}. && (43)\end{aligned}$$

On the other hand, this implies that, in a finite amount of time, one has $\sigma = 0$, and the trajectories of system (8) will converge to zero in FnT as well, under $\sigma = 0$. In fact, if $\sigma = 0$ holds in (16), the sliding variable will converge to zero in a FnT according to Lemma 2, i.e.,

$$\begin{aligned} \sigma &= \mathcal{S} + \Lambda D^{\beta-1}\mathcal{S}_{I\beta} = 0\\ D^{\beta}\mathcal{S}_{I\beta} &= \mathrm{sig}\left(\mathcal{S}\right)^{\alpha}. \end{aligned} \tag{44}$$

Hence, one has

$$\begin{aligned} D^{\beta}\mathcal{S}_{I\beta} &= \mathrm{sig}\left(\Lambda D^{\beta-1}\mathcal{S}_{I\beta}\right)^{\alpha}\\ &= -\Lambda^{\alpha}D^{\beta-1}\mathrm{sig}^{\alpha}\left(\mathcal{S}_{I\beta}\right), \end{aligned} \tag{45}$$

which, after a simple calculation, implies

$$\dot{S}_{I\beta} = -\Lambda^{\alpha}\mathrm{sig}^{\alpha}\left(S_{I\beta}\right). \tag{46}$$

Finally, making reference to Lemma 2, the convergence time t_s is given by

$$t_s = \frac{|\sigma(0)|^{1-\alpha}}{\Lambda(1-\alpha)}. \tag{47}$$

□

Remark 2. The control signal (22) is the same as a fractional-order high-pass filter (FOHPF), with $\varepsilon(t)$ as the input and $\mathcal{U}_1$ as the filter's output. The fractional-order filter's Laplace transfer function (22) is given by

$$\frac{\mathcal{U}_1(t)}{\varepsilon(t)} = \frac{s^{\lambda-1}}{s^{\lambda}+\mathcal{T}}, \tag{48}$$

where $\mathcal{T}$ is the FOHPF's bandwidth, while $\mathcal{U}_1(t)$ in (20) is the output of the FOHPF (22) which is softened to be a smooth signal by the switch function, despite the fact that $\varepsilon(t)$ is non-smooth due to the switching function (22).

Remark 3. The disadvantage of the strategies proposed in [9,12,10] is that the reaching phase is still present. The reaching phase is instead removed in our method due to the proposed recursive fractional-order integral terminal sliding manifold, and the system begins to move on the sliding surface since the initial time instant. Moreover, the proposal exhibits certain noteworthy characteristics with respect to existing methods in [9,12,10], which are outlined as follows:

- First, for the existing nonsingular terminal sliding manifold [9,12,10], the designed surface variable following the non-recursive manner can only admit an existence condition for FnT stability.
- It can be seen from the existing works [12,17,32] that the proposed FORITSM offers an additional degree of freedom, due to the designed FO filter.

4 | APPLICATION TO TRACKING CONTROL FOR A QUADROTOR UAV

In this section, the proposed control approach is applied to the dynamics of a quadrotor UAV, showing its applicability in a practical case.

4.1 | Modelling and tracking control problem

Consider a quadrotor system [33] captured by the following equations

$$\begin{aligned}
\ddot{\phi} &= \dot{\theta}\dot{\psi}\frac{(J_{YY}-J_{ZZ})}{J_{XX}} - \frac{I_{rr}}{J_{XX}}\Omega_r\dot{\theta} - \frac{\vartheta_{\phi}}{J_{XX}}\dot{\phi}^2 + \frac{1}{J_{XX}}\tau_{\phi} + \mathcal{D}_{\phi}\\
\ddot{\theta} &= \dot{\phi}\dot{\psi}\frac{(J_{ZZ}-J_{XX})}{J_{YY}} + \frac{I_{rr}}{J_{YY}}\Omega_r\dot{\phi} - \frac{\vartheta_{\theta}}{J_{YY}}\dot{\theta}^2 + \frac{1}{J_{YY}}\tau_{\theta} + \mathcal{D}_{\theta}\\
\ddot{\psi} &= \dot{\phi}\dot{\theta}\frac{(J_{XX}-J_{YY})}{J_{ZZ}} - \frac{\vartheta_{\psi}}{J_{ZZ}}\dot{\psi}^2 + \frac{1}{J_{ZZ}}\tau_{\psi} + \mathcal{D}_{\psi}\\
\ddot{x} &= -\frac{\vartheta_x}{m}\dot{x} + (\cos\phi\sin\theta\cos\psi + \sin\phi\sin\psi)\frac{T}{m} + \mathcal{D}_x\\
\ddot{y} &= -\frac{\vartheta_y}{m}\dot{y} + (\cos\phi\sin\theta\sin\psi - \sin\phi\cos\psi)\frac{T}{m} + \mathcal{D}_y\\
\ddot{z} &= -\frac{\vartheta_z}{m}\dot{z} - g + (\cos\phi\cos\theta)\frac{T}{m} + \mathcal{D}_z,
\end{aligned} \tag{49}$$

where the Euler angles of the quadrotor are expressed as $\Upsilon_{\eta} = [\phi\ \theta\ \psi]^T$, and $\dot{\Upsilon}_{\eta} = [\dot{\phi}\ \dot{\theta}\ \dot{\psi}]^T$ are the angular rates. As shown in Fig. (1), the absolute position of the the quadrotor is $\Upsilon_q = [x\ y\ z]^T$, and $\dot{\Upsilon}_q = [\dot{x}\ \dot{y}\ \dot{z}]^T$ represents the linear velocity, where J_{XX}, J_{YY}, and J_{ZZ} are inertia moments of the vehicle around b_x, b_y, b_z axes, m is the mass of the body, $\mathcal{D}_{\phi}$, $\mathcal{D}_{\theta}$, $\mathcal{D}_{\psi}$, $\mathcal{D}_x$, $\mathcal{D}_y$ and $\mathcal{D}_z$ denote the external disturbances, and g is the gravitational acceleration. Moreover, $\vartheta_i|_{x,y,z,\phi,\theta,\psi}$ are drag coefficients, and

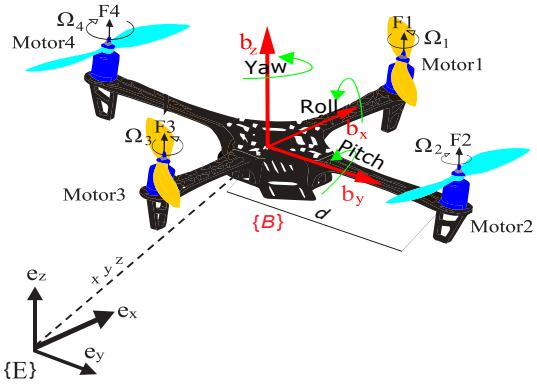

FIGURE 1 Quadrotor configuration.

$[T\ \tau_\phi\ \tau_\theta\ \tau_\psi]^T$ are the control inputs. In order to generate the total thrust T and the tilting angles (ϕ_d, θ_d), the virtual control input can be defined as follows

$$P_x = (\cos\phi \sin\theta \cos\psi + \sin\phi \sin\psi)\frac{T}{m} \tag{50}$$

$$P_y = (\cos\phi \sin\theta \sin\psi - \sin\phi \cos\psi)\frac{T}{m} \tag{51}$$

$$P_z = -g + (\cos\phi \cos\theta)\frac{T}{m}. \tag{52}$$

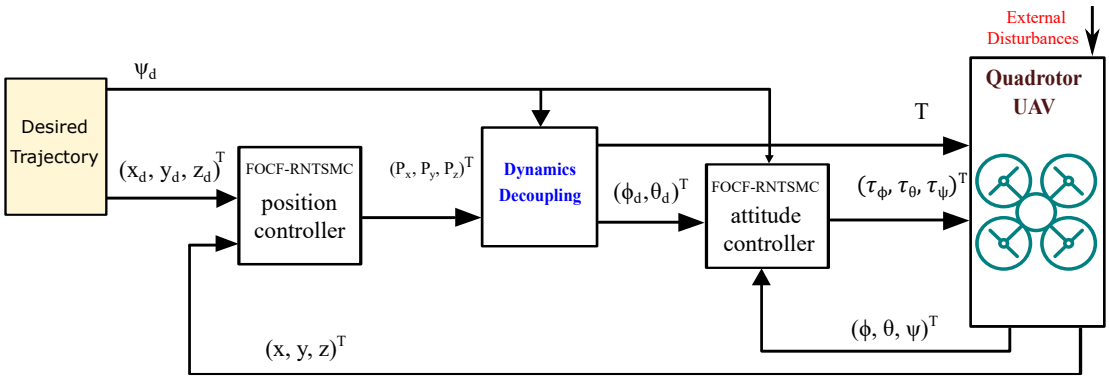

FIGURE 2 The proposed control scheme for the quadrotor UAV.

We are now in a position to formulate the considered tracking control problem. Specifically, the control objective is to design a FORITSM control for the system (49) in order to make the quadrotor follow a reference trajectory. In this context, the virtual signal $P_i = [P_x,\ P_y,\ P_z]^T$ will be designed in order to generate the total thrust T, the titling anglers (ϕ_d, θ_d) for the outer loop, and the torque controls $(\tau_\phi, \tau_\theta, \tau_\psi)$, as shown in Fig. (2).

4.2 | FORITSM control design for the quadrotor

Let us define the tracking errors and their derivatives for the quadrotor position as follows

$$\mathbf{e}_x = x - x_d, \quad \mathbf{e}_x = \ y - y_d, \quad \mathbf{e}_z = z - x_d \tag{53}$$

and

$$\dot{\mathbf{e}}_x = \dot{x} - \dot{x}_d, \quad \dot{\mathbf{e}}_x = \ \dot{y} - \dot{y}_d, \quad \dot{\mathbf{e}}_z = \dot{z} - \dot{x}_d \tag{54}$$

Similarly, the tracking errors and their derivatives are defined for the attitude as follows

$$\mathbf{e}_{\phi} = \phi - \phi_d, \quad \mathbf{e}_{\theta} = \theta - \theta_d, \quad \mathbf{e}_{\psi} = \psi - \psi_d \tag{55}$$

and

$$\dot{\mathbf{e}}_{\phi} = \dot{\phi} - \dot{\phi}_d, \quad \dot{\mathbf{e}}_{\theta} = \dot{\theta} - \dot{\theta}_d, \quad \dot{\mathbf{e}}_{\psi} = \dot{\psi} - \dot{\psi}_d \tag{56}$$

Now, in order to design the proposed FORITSM control, the fast nonsingular terminal sliding manifolds for the position need to be defined as

$$\mathcal{S}_x = \ddot{\mathbf{e}}_x + \kappa_{2x}\text{sign}\left(\dot{\mathbf{e}}_x\right)\left|\dot{\mathbf{e}}_x\right|^{\mu_{x2}} + \kappa_{x1}\text{sign}\left(\mathbf{e}_x\right)\left|\mathbf{e}_x\right|^{\mu_{x1}} \tag{57}$$

$$\mathcal{S}_y = \ddot{\mathbf{e}}_y + \kappa_{2y}\text{sign}\left(\dot{\mathbf{e}}_y\right)\left|\dot{\mathbf{e}}_y\right|^{\mu_{y2}} + \kappa_{y1}\text{sign}\left(\mathbf{e}_y\right)\left|\mathbf{e}_y\right|^{\mu_{y1}} \tag{58}$$

$$\mathcal{S}_z = \ddot{\mathbf{e}}_z + \kappa_{2z}\text{sign}\left(\dot{\mathbf{e}}_z\right)\left|\dot{\mathbf{e}}_z\right|^{\mu_{x2}} + \kappa_{z1}\text{sign}\left(\mathbf{e}_z\right)\left|\mathbf{e}_z\right|^{\mu_{z1}}. \tag{59}$$

The fast nonsingular terminal sliding manifolds for the attitude are instead given by

$$\mathcal{S}_{\phi} = \ddot{\mathbf{e}}_{\phi} + \kappa_{2\phi}\text{sign}\left(\dot{\mathbf{e}}_{\phi}\right)\left|\dot{\mathbf{e}}\phi\right|^{\mu_{\phi 2}} + \kappa_{\phi 1}\text{sign}\left(\mathbf{e}_{\phi}\right)\left|\mathbf{e}_{\phi}\right|^{\mu_{\phi 1}} \tag{60}$$

$$\mathcal{S}_{\theta} = \ddot{\mathbf{e}}_{\theta} + \kappa_{2\theta}\text{sign}\left(\dot{\mathbf{e}}_{\theta}\right)\left|\dot{\mathbf{e}}_{\theta}\right|^{\mu_{\theta 2}} + \kappa_{\theta 1}\text{sign}\left(\mathbf{e}_{\theta}\right)\left|\mathbf{e}_{\theta}\right|^{\mu_{\theta 1}} \tag{61}$$

$$\mathcal{S}_{\psi} = \ddot{\mathbf{e}}_{\psi} + \kappa_{2\psi}\text{sign}\left(\dot{\mathbf{e}}_{\psi}\right)\left|\dot{\mathbf{e}}_{\psi}\right|^{\mu_{\psi 2}} + \kappa_{\psi 1}\text{sign}\left(\mathbf{e}_{\psi}\right)\left|\mathbf{e}_{\psi}\right|^{\mu_{\psi 1}}. \tag{62}$$

The control parameters μ_{i1} and μ_{i1} for $(i = x, y, z, \phi, \theta, \psi)$ are selected according to Lemma 1, while κ_{i1} and κ_{i2} are positive coefficients.

The fractional-order integral terminal sliding manifolds for the position and attitude are respectively

$$\sigma_x = \mathcal{S}_x + \Lambda_x D^{\beta_x - 1}\mathcal{S}_{I\beta_x}, \quad \sigma_y = \mathcal{S}_y + \Lambda_y D^{\beta_y - 1}\mathcal{S}_{I\beta_y}, \quad \sigma_z = \mathcal{S}_z + \Lambda_z D^{\beta_z - 1}\mathcal{S}_{I\beta_z}, \tag{63}$$

and

$$\sigma_{\phi} = \mathcal{S}_{\phi} + \Lambda_{\phi} D^{\beta_{\phi} - 1}\mathcal{S}_{I\beta_{\phi}}, \quad \sigma_{\theta} = \mathcal{S}_{\theta} + \Lambda_{\theta} D^{\beta_{\theta} - 1}\mathcal{S}_{I\beta_{\theta}}, \quad \sigma_{\psi} = \mathcal{S}_{\psi} + \Lambda_{\psi} D^{\beta_{\psi} - 1}\mathcal{S}_{I\beta_{\psi}}, \tag{64}$$

where Λ_i are positive coefficients and $\mathcal{S}_i$ as in (57) and (62), while $\mathcal{S}_{I\beta_i}$ can be designed as

$$D^{\beta_x}\mathcal{S}_{I\beta_x} = \text{sig}\left(\mathcal{S}_x\right)^{\alpha_x}, \quad D^{\beta_y}\mathcal{S}_{I\beta_y} = \text{sig}\left(\mathcal{S}_y\right)^{\alpha_y}, \quad D^{\beta_z}\mathcal{S}_{I\beta_z} = \text{sig}\left(\mathcal{S}_z\right)^{\alpha_z}, \tag{65}$$

and

$$D^{\beta_{\phi}}\mathcal{S}_{I\beta_{\phi}} = \text{sig}\left(\mathcal{S}_{\phi}\right)^{\alpha_{\phi}}, \quad D^{\beta_{\theta}}\mathcal{S}_{I\beta_{\theta}} = \text{sig}\left(\mathcal{S}_{\theta}\right)^{\alpha_{\theta}}, \quad D^{\beta_{\psi}}\mathcal{S}_{I\beta_{\psi}} = \text{sig}\left(\mathcal{S}_{\psi}\right)^{\alpha_{\psi}}. \tag{66}$$

Assumption 2. The function $\mathcal{D}_i$ is assumed to be unknown, but its amplitude and derivative are bounded so that $\mathcal{D}_i < \Upsilon_{Ti}$ and $\dot{\mathcal{D}}_i < \Upsilon_{di}$.

Theorem 3. Given the quadrotor dynamics (49), controlled via the FORITSM control laws (67)-(84), that is, for the x-subsystem

$$P_x = \left(P_{x0} + P_{x1}\right) \tag{67}$$

$$P_{x0} = -\frac{\vartheta_x}{m}\dot{x} - \kappa_{2x}\text{sign}\left(\dot{\mathbf{e}}_x\right)\left|\dot{\mathbf{e}}_x\right|^{\mu_{x2}} - \kappa_{x1}\text{sign}\left(\mathbf{e}_x\right)\left|\mathbf{e}_x\right|^{\mu_{x1}} - \Lambda_x D^{\beta_x}\mathcal{S}_{I\beta_x} \tag{68}$$

$$D^{\lambda_x}P_{x1} + \mathcal{T}_x P_{x1} = \varsigma_x,$$
$$\varsigma_x = -\left(\Upsilon_{dx} + \Upsilon_{Tx} + \varsigma_{x0}\right)D^{\lambda_x - 1}\text{sign}(\sigma_x) - K_{fx}D^{\lambda_x - 1}\sigma_x, \tag{69}$$

for the y-subsystem

$$P_y = \left(P_{y0} + P_{y1}\right) \tag{70}$$

$$P_{y0} = -\frac{\vartheta_y}{m}\dot{y} - \kappa_{2y}\text{sign}\left(\dot{\mathbf{e}}_y\right)\left|\dot{\mathbf{e}}_y\right|^{\mu_{y2}} - \kappa_{y1}\text{sign}\left(\mathbf{e}_y\right)\left|\mathbf{e}_y\right|^{\mu_{y1}} - \Lambda_y D^{\beta_y}\mathcal{S}_{I\beta_y} \tag{71}$$

$$D^{\lambda_y}P_{x1} + \mathcal{T}_y P_{y1} = \varsigma_y,$$
$$\varsigma_y = -\left(\Upsilon_{dy} + \Upsilon_{Ty} + \varsigma_{y0}\right)D^{\lambda_y - 1}\text{sign}(\sigma_y) - K_{fy}D^{\lambda_y - 1}\sigma_y, \tag{72}$$

for the z-subsystem

$$P_z = \left(P_{z0} + P_{z1}\right) \tag{73}$$

$$P_{z0} = -\frac{\vartheta_z}{m}\dot{z} + g - \kappa_{2z}\text{sign}\left(\dot{\mathbf{e}}_z\right)\left|\dot{\mathbf{e}}_z\right|^{\mu_{z2}} - \kappa_{z1}\text{sign}\left(\mathbf{e}_z\right)\left|\mathbf{e}_z\right|^{\mu_{z1}} - \Lambda_z D^{\beta_z} S_{I\beta_z} \tag{74}$$

$$D^{\lambda_z} P_{z1} + \mathcal{T}_z P_{z1} = \varsigma_z,$$
$$\varsigma_z = -\left(\Upsilon_{dz} + \Upsilon_{Tz} + \varsigma_{z0}\right) D^{\lambda_z - 1}\text{sign}(\sigma_z) - K_{fz} D^{\lambda_z - 1}\sigma_z, \tag{75}$$

for the ϕ-subsystem

$$\tau_\phi = J_{XX}\left(\tau_{\phi 0} + \tau_{\phi 1}\right) \tag{76}$$

$$\tau_{\phi 0} = -\{\dot{\theta}\dot{\psi}\frac{(J_{YY} - J_{ZZ})}{J_{XX}} - \frac{I_{rr}}{J_{XX}}\Omega_r\dot{\theta} - \frac{\vartheta_\phi}{J_{XX}}\dot{\phi}^2\} - \kappa_{2\phi}\text{sign}\left(\dot{\mathbf{e}}_\phi\right)\left|\dot{\mathbf{e}}_\phi\right|^{\mu_{\phi 2}} - \kappa_{\phi 1}\text{sign}\left(\mathbf{e}_\phi\right)\left|\mathbf{e}_\phi\right|^{\mu_{\phi 1}} - \Lambda_\phi D^{\beta_\phi} S_{I\beta_\phi} \tag{77}$$

$$D^{\lambda_\phi}\tau_{\phi 1} + \mathcal{T}_\phi\tau_{\phi 1} = \varsigma_\phi,$$
$$\varsigma_\phi = -\left(\Upsilon_{d\phi} + \Upsilon_{T\phi} + \varsigma_{\phi 0}\right) D^{\lambda_\phi - 1}\text{sign}(\sigma_\phi) - K_{f\phi} D^{\lambda_\phi - 1}\sigma_\phi, \tag{78}$$

for the θ-subsystem

$$\tau_\theta = J_{YY}\left(\tau_{\theta 0} + \tau_{\theta 1}\right) \tag{79}$$

$$\tau_{\theta 0} = -\{\dot{\phi}\dot{\psi}\frac{(J_{ZZ} - J_{XX})}{J_{YY}} + \frac{I_{rr}}{J_{YY}}\Omega_r\dot{\phi} - \frac{\vartheta_\theta}{J_{YY}}\dot{\theta}^2\} - \kappa_{2\theta} sign\left(\dot{\mathbf{e}}_\theta\right)\left|\dot{\mathbf{e}}_\theta\right|^{\mu_{\theta 2}} - \kappa_{\theta 1}\text{sign}\left(\mathbf{e}_\theta\right)\left|\mathbf{e}_\theta\right|^{\mu_{\theta 1}} - \Lambda_\theta D^{\beta_\theta} S_{I\beta_\theta} \tag{80}$$

$$D^{\lambda_\theta}\tau_{\theta 1} + \mathcal{T}_\theta\tau_{\theta 1} = \varsigma_\theta,$$
$$\varsigma_\theta = -\left(\Upsilon_{d\theta} + \Upsilon_{T\theta} + \varsigma_{\theta 0}\right) D^{\lambda_\theta - 1}\text{sign}(\sigma_\theta) - K_{f\theta} D^{\lambda_i heta - 1}\sigma_\theta, \tag{81}$$

for the ψ-subsystem

$$\tau_\psi = J_{ZZ}\left(\tau_{\psi 0} + \tau_{\psi 1}\right) \tag{82}$$

$$\tau_{\psi 0} = -\{\dot{\phi}\dot{\theta}\frac{(J_{XX} - J_{YY})}{J_{ZZ}} - \frac{\vartheta_\psi}{J_{ZZ}}\dot{\psi}^2\} - \kappa_{2\psi} sign\left(\dot{\mathbf{e}}_\psi\right)\left|\dot{\mathbf{e}}_\psi\right|^{\mu_{\psi 2}} - \kappa_{\psi 1}\text{sign}\left(\mathbf{e}_\psi\right)\left|\mathbf{e}_\psi\right|^{\mu_{\psi 1}} - \Lambda_\psi D^{\beta_\psi} S_{I\beta_\psi} \tag{83}$$

$$D^{\lambda_\psi}\tau_{\psi 1} + \mathcal{T}_\psi\tau_{\psi 1} = \varsigma_\psi,$$
$$\varsigma_\psi = -\left(\Upsilon_{d\psi} + \Upsilon_{T\psi} + \varsigma_{\psi 0}\right) D^{\lambda_\psi - 1}\text{sign}(\sigma_\psi) - K_{f\psi} D^{\lambda_\psi - 1}\sigma_\psi, \tag{84}$$

where $\kappa_{i1}, \kappa_{i2} > 0$, $\Upsilon_{di}, \Upsilon_{Ti}$, and ς_{0i} are positive constants, λ_i is fractional operator, and Υ_{di} and Υ_{Ti} are two constants, if $\Upsilon_{Ti} > \mathcal{T}_i\delta_i$, then σ_x, σ_y, σ_z, σ_ϕ,σ_θ, and σ_ψ are zeroed in a finite time. Moreover, the position and attitude dynamics in (49) are regulated to their references in a finite time, constrained to the sliding mode on $\sigma_x = \sigma_y = \sigma_z = \sigma_\phi = \sigma_\theta = \sigma_\psi = 0$.

Proof. Taking into account the sliding manifolds in (57), (62), and substituting the proposed control laws (67)-(84) to (63), (64), one has

$$\sigma_x = P_{x1} + \mathcal{D}_x, \quad \sigma_y \quad P_{y1} + \mathcal{D}_y, \quad \sigma_z = P_{z1} + \mathcal{D}_z, \tag{85}$$

and

$$\sigma_\phi = \tau_{\phi 1} + \mathcal{D}_\phi, \quad \sigma_\theta = \quad \tau_{\theta 1} + \mathcal{D}_\theta, \quad \sigma_\psi = \tau_{\psi 1} + \mathcal{D}_\psi. \tag{86}$$

Using the results of the Theorem 2, the solutions of the control inputs (69), (72), (75), (78), (81), and (84) are

$$P_{y1}(t) = P_{x1}(0)t^{-\lambda_x}E_{-\lambda_x,-\lambda_x+1}\left(-\mathcal{T}_x t^{-\lambda_x}\right) + P_{x1}(0)E_{-\lambda_x}\left(-\mathcal{T}_x t^{-\lambda_x}\right) + \int_0^t \left(t-\tau\right)^{-\lambda_x} E_{-\lambda_x,-\lambda_x+1}\left(-\mathcal{T}_x\left(t-\tau\right)^{-\lambda_x}\right)\zeta_x(\tau)d\tau \tag{87}$$

$$P_{y1}(t) = P_{y1}(0)t^{-\lambda_y}E_{-\lambda_y,-\lambda_y+1}\left(-\mathcal{T}_y t^{-\lambda_y}\right) + P_{x1}(0)E_{-\lambda_y}\left(-\mathcal{T}_y t^{-\lambda_y}\right) + \int_0^t \left(t-\tau\right)^{-\lambda_y} E_{-\lambda_y,-\lambda_y+1}\left(-\mathcal{T}_y\left(t-\tau\right)^{-\lambda_y}\right)\zeta_y(\tau)d\tau \tag{88}$$

$$P_{z1}(t) = P_{z1}(0)t^{-\lambda_z}E_{-\lambda_z,-\lambda_z+1}\left(-\mathcal{T}_z t^{-\lambda_z}\right) + P_{x1}(0)E_{-\lambda_z}\left(-\mathcal{T}_z t^{-\lambda_z}\right) + \int_0^t \left(t-\tau\right)^{-\lambda_z} E_{-\lambda_z,-\lambda_z+1}\left(-\mathcal{T}_z\left(t-\tau\right)^{-\lambda_z}\right)\zeta_z(\tau)d\tau \tag{89}$$

$$\tau_{\phi 1}(t) = \tau_{\phi 1}(0)t^{-\lambda_\phi} E_{-\lambda_\phi,-\lambda_\phi+1}\left(-\mathcal{T}_\phi t^{-\lambda_\phi}\right) + P_{x1}(0)E_{-\lambda_\phi}\left(-\mathcal{T}_\phi t^{-\lambda_\phi}\right) + \int_0^t \left(t-\tau\right)^{-\lambda_\phi} E_{-\lambda_\phi,-\lambda_\phi+1}\left(-\mathcal{T}_\phi \left(t-\tau\right)^{-\lambda_\phi}\right)\zeta_\phi(\tau)d\tau \tag{90}$$

$$\tau_{\theta 1}(t) = \tau_{\theta 1}(0)t^{-\lambda_\theta} E_{-\lambda_\theta,-\lambda_\theta+1}\left(-\mathcal{T}_\theta t^{-\lambda_\theta}\right) + P_{x1}(0)E_{-\lambda_\theta}\left(-\mathcal{T}_\theta t^{-\lambda_\theta}\right) + \int_0^t \left(t-\tau\right)^{-\lambda_\theta} E_{-\lambda_\theta,-\lambda_\theta+1}\left(-\mathcal{T}_\theta \left(t-\tau\right)^{-\lambda_\theta}\right)\zeta_\theta(\tau)d\tau \tag{91}$$

$$\tau_{\psi 1}(t) = \tau_{\psi 1}(0)t^{-\lambda_\psi} E_{-\lambda_\psi,-\lambda_\psi+1}\left(-\mathcal{T}_\psi t^{-\lambda_\psi}\right) + P_{x1}(0)E_{-\lambda_\psi}\left(-\mathcal{T}_\psi t^{-\lambda_\psi}\right) + \int_0^t \left(t-\tau\right)^{-\lambda_\psi} E_{-\lambda_\psi,-\lambda_\psi+1}\left(-\mathcal{T}_\psi \left(t-\tau\right)^{-\lambda_\psi}\right)\zeta_\psi(\tau)d\tau \tag{92}$$

Using the condition $\Upsilon_{Ti} > \mathcal{T}_i\delta_i$ and from (24) and (87)-(92), under the condition $P_x(0) = P_y(0) = P_z(0) = \tau_\phi(0) = \tau_\theta(0) = \tau_\psi = 0$ one obtains $\Upsilon_{Ti} \geq \mathcal{T}_i$, $\Upsilon_{di} \geq \mathcal{T}_i \left|P_{x1}, P_{y1}, P_{z1}, \tau_{\phi 1}, \tau_{\theta 1}, \tau_{\psi 1}\right|_{\max} \geq \mathcal{T}_i \left|P_{x1}, P_{y1}, P_{z1}, \tau_{\phi 1}, \tau_{\theta 1}, \tau_{\psi 1}\right|$, i.e., $\mathcal{T}_i \left|P_{x1}, P_{y1}, P_{z1}, \tau_{\phi 1}, \tau_{\theta 1}, \tau_{\psi 1}\right| \leq \Upsilon_{Ti}$.

Consider now the global Lyapunov function for overall quadrotor system $\mathcal{V}_g = \frac{1}{2}\left[\sigma_x^2 + \sigma_y^2 + \sigma_z^2 + \sigma_\phi^2 + \sigma_\theta^2 + \sigma_\psi^2.\right]$ The FO derivative of terminal sliding manifold is

$$\begin{aligned} D^{\lambda_i}\sigma_i &= D^{\lambda_i}\mathcal{D}_i + D^{\lambda_i}\Gamma && (93)\\ &= D^{\lambda_i}\mathcal{D}_i + D_i^{\lambda}\Gamma + \mathcal{T}_i\Gamma - \mathcal{T}_i\Gamma && (94)\\ &= D^{\lambda_i}\mathcal{D}_i + \zeta_i - \mathcal{T}_i\Gamma && (95)\\ &= D^{\lambda_i}\mathcal{D}_i - D^{\lambda_i - 1}\left[\left(\Upsilon_{di} + \Upsilon_{Ti} + \varsigma_{0i}\right)\text{sign}(\sigma_i) - K_{fi}\sigma_i\right] - \mathcal{T}_i\Gamma. && (96)\end{aligned}$$

with Γ representing the input controls $P_x, P_y, P_z, \tau_\phi, \tau_\theta, \tau_\psi$. Hence,

$$\begin{aligned} \sigma_i\dot{\sigma}_i &= \dot{\mathcal{D}}_i\sigma_i - \left(\Upsilon_{di} + \Upsilon_{Ti} + \varsigma_{0i}\right)\left|\sigma_i\right| - K_{fi}\sigma_i^2 - \mathcal{T}_i D^{1-\lambda_i}\Gamma\sigma_i && (97)\\ &\leq \left|\dot{\mathcal{D}}_i\right|\left|\sigma_i\right| - \Upsilon_{di}\left|\sigma_i\right| + \left[-\mathcal{T}_i D^{1-\lambda_i}\Gamma\sigma_i - \Upsilon_{Ti}\left|\sigma_i\right|\right] - \varsigma_{0i}\left|\sigma_i\right| - K_{fi}\sigma_i^2 && (98)\end{aligned}$$

According to Assumption (2) and exploiting (97), one has

$$\begin{aligned} \dot{\mathcal{V}}_g &= \sigma_x\dot{\sigma}_x + \sigma_y\dot{\sigma}_y + \sigma_z\dot{\sigma}_z + \sigma_\phi\dot{\sigma}_\phi + \sigma_\theta\dot{\sigma}_\theta + \sigma_\psi\dot{\sigma}_\psi && (99)\\ &\leq -\Big(\sum_{i=x,y,z,\phi,\theta,\psi} \varsigma_{0i}\left|\sigma_i\right| + K_{fi}\sigma_i^2\Big) < 0. && (100)\end{aligned}$$

This implies that $\sigma_i = 0$ in a FnT, as well as the quadrotor system trajectories will converge to zero in FnT, under $\sigma_i = 0$. □

5 | SIMULATION RESULTS

In this section, realistic simulation results are illustrated to assess the proposed control approach, even in comparison with the control law proposed in [12].

5.1 | Settings

In the following a wide simulation campaign is discussed. More specifically, the following scenarios are considered:

Nominal model: In this scenario the proposed FORITSM control for position tracking is considered by using nominal parameters of the quadrotor. In addition, the simulation results of the proposed controller are compared with those achieve by using the control law in [12].

Increasing disturbance amplitudes: In this scenario the proposed controller and the controller proposed in [12] are tested considering the disturbances in (101) and (102) applied respectively for position and attitude of the quadrotor, by increasing

their amplitudes with respect to time:

$$\begin{aligned}
\mathcal{D}_x &= \sin(4t) + \cos(4t),\ t \in [0, \pi] \\
\mathcal{D}_x &= 1.3\sin(4t) + 1.3\cos(4t),\ t \in]\pi, 80] \\
\mathcal{D}_y &= \sin(5t) + \cos(5t),\ t \in [0, \frac{5}{7}\pi] \\
\mathcal{D}_y &= 1.1\sin(5t) + 1.4\cos(5t),\ t \in]\tfrac{5}{7}\pi, 80] \\
\mathcal{D}_z &= \sin(5t) + \cos(5t),\ t \in [0, 2\pi] \\
\mathcal{D}_z &= 2\sin(4t) + 2\cos(5t),\ t \in]2\pi, 80]
\end{aligned} \tag{101}$$

and

$$\begin{aligned}
\mathcal{D}_\phi &= 1.3\sin(5t) + 1.3\cos(5t),\ t \in [0, 2\pi] \\
\mathcal{D}_\phi &= 4\sin((5t) + 4\cos(5t),\ t \in]2\pi, 80] \\
\mathcal{D}_\theta &= 1.6\sin(5t) + 1.6\cos(5t),\ t \in [0, 2\pi] \\
\mathcal{D}_\theta &= 4\sin(5t) + 4\cos(5t),\ t \in]2\pi, 80] \\
\mathcal{D}_\phi &= 1.5\sin(5t) + 2\cos(5t),\ t \in [0, 2\pi] \\
\mathcal{D}_\phi &= 5\sin(4t) + 5\cos(5t),\ t \in]2\pi, 80].
\end{aligned} \tag{102}$$

Increasing disturbance frequencies: In this scenario the proposed control method and the controller proposed in [12] are tested considering the disturbances in (103) and (104) applied respectively for position and attitude of the quadrotor, by increasing their frequencies with respect to time.

$$\begin{aligned}
\mathcal{D}_x &= \sin(4t) + \cos(4t),\ t \in [0, \pi] \\
\mathcal{D}_x &= \sin(40t) + \cos(40t),\ t \in]\pi, 80] \\
\mathcal{D}_y &= \sin(5t) + \cos(5t),\ t \in [0, \frac{5}{7}\pi] \\
\mathcal{D}_y &= \sin(50t) + \cos(50t),\ t \in]\frac{5}{7}\pi, 80] \\
\mathcal{D}_z &= \sin(5t) + \cos(5t),\ t \in [0, 2\pi] \\
\mathcal{D}_z &= \sin(100t) + \cos(100t),\ t \in]2\pi, 80]
\end{aligned} \tag{103}$$

and

$$\begin{aligned}
\mathcal{D}_\phi &= 3\sin(5t) + 3\cos(5t),\ t \in [0, 2\pi] \\
\mathcal{D}_\phi &= \sin((100t) + \cos(100t),\ t \in]2\pi, 80] \\
\mathcal{D}_\theta &= 1.6\sin(5t) + 1.6\cos(5t),\ t \in [0, 2\pi] \\
\mathcal{D}_\theta &= 1.6\sin(5t) + 1.6\cos(5t),\ t \in]2\pi, 80] \\
\mathcal{D}_\psi &= 5\sin(100t) + 2\cos(100t),\ t \in [0, 2\pi] \\
\mathcal{D}_\psi &= \sin(100t) + \cos(100t),\ t \in]2\pi, 80]
\end{aligned} \tag{104}$$

The quadrotor parameters for the considered scenarios are reported in Table 1, while the control parameters are given by $\mu_{i1} = \frac{9}{16}$, $\mu_{i2} = \frac{9}{23}$, $\alpha_{i1} = 0.2$, $\beta_{i2} = 72$, $\Lambda_1 = 0.05$, $\epsilon_{0i} = 0.5$, $\kappa_{2i} = 72$, $\kappa_{1i} = 192$, $\Upsilon_{di} = 14$, and $\Upsilon_{Ti} = 2.4$.

5.2 | Nominal model

Now the first scenario in nominal conditions is discussed. Fig. 3 shows the reference position tracking results. It can be observed that, by using the proposed method, fast and precise trajectory tracking is achieved, differently from the case when the method proposed in [12] is adopted. Indeed, the latter determines a big overshoot in the position outputs. The tracking performance of the attitude is instead plotted in Fig. 4, with satisfactory results when using the proposal. The tracking errors including $\mathbf{e}_x$, $\mathbf{e}_y$, $\mathbf{e}_z$, and $\mathbf{e}_\psi$ are zeroed as expected and displayed in Fig. 5. The results of the tracking in 2D and 3D environments are plotted respectively in Fig. 6 and Fig. 7. Fig. 8 finally shows the results of the control inputs whose amplitudes are small and converge to their nominal values.

TABLE 1 Quadrotor parameters.

Parameter	Value	Parameter	Value
$g(s{-}^2.m)$	9.8	ϑ_y (Nms^2)	0.01
$m(kg)$	0.486	ϑ_z (Nms^2)	0.01
$J_{XX}(m{-}^2.kg)$	3.8278e-3	$\vartheta_\phi(Nrads^2)$	0.012
$J_{YY}(m{-}^2.kg)$	3.8278e-3	$\vartheta_\theta(Nrads^2)$	0.012
$J_{ZZ}(m{-}^2.kg)$	7.6566e-3	$\vartheta_\psi(Nrads^2)$	0.012
$I_{rr}(m{-}^2.kg)$	2.8385e-5	$b_\aleph(N.s^2)$	2.9842e-3
ϑ_x (Nms^2)	0.01	$c_d(N.m.s^2)$	3.2320e-2

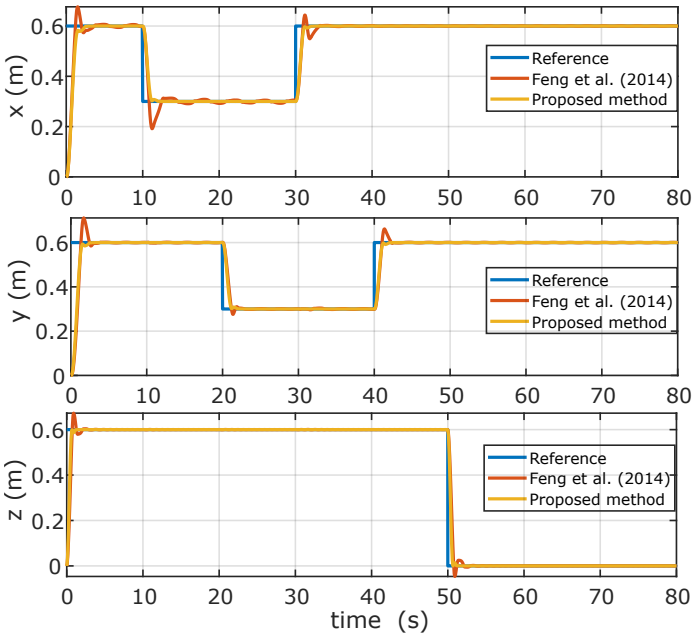

FIGURE 3 Simulation results showing the position performance of each controller: reference (—), control in Feng et al. (2014) (—), and proposed method (—) (Nominal model).

5.3 | Increasing disturbance amplitudes

The results of the second scenario are now discussed. It can be seen that the proposed controller drives the outputs to converge to their desired trajectories in FnT. Moreover, the negative effect caused by the presence of the disturbances is removed. On the other hand, it can be noticed that the results provided by the control law in [12] are less satisfactory than the ones achieved via the proposed method, see, for example, Fig. 9 where high oscillation are present. The attitude and tracking errors are plotted respectively in Fig. 10 and 11. Again, it can be observed that the attitude and tracking errors are zeroed. Finally, Figs. 12 and 13 show that the proposed controller allows to achieve a good tracking performance compared to [12]. The amplitudes of the inputs presented in Fig. 14 are small and with a reduced chattering phenomenon.

5.4 | Increasing disturbance frequencies

The results of the third scenario are illustrated hereafter. In terms of the convergence rate, rejection of the disturbances, and tracking performance, the proposed controller outperforms the one in [12] as shown in Figs. 15 and 16 for position and attitude respectively, as well as in terms of tracking errors. In fact, the proposed approach ensures fast convergence rate with lower

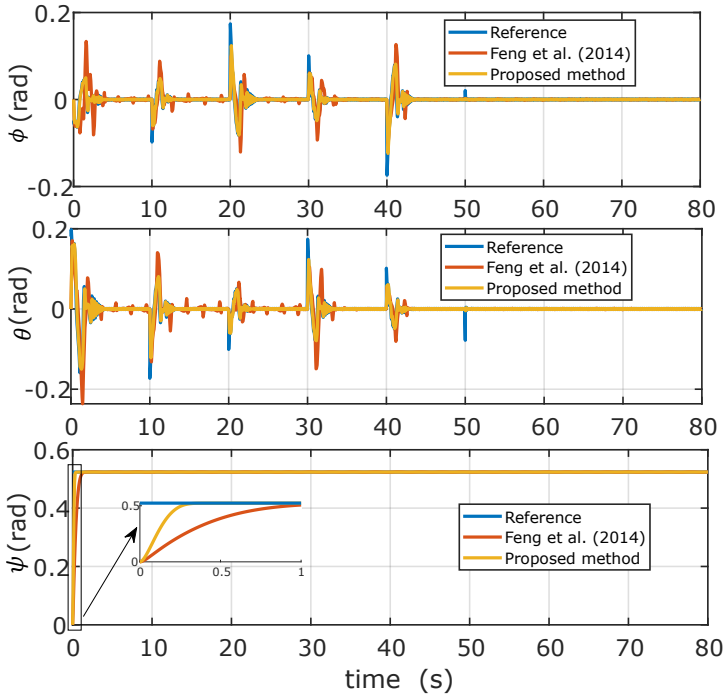

FIGURE 4 Simulation results showing the attitude performance of each controller: reference (—), control in Feng et al. (2014) (—), and proposed method (—) (Nominal model).

undershoot of the system-controlled outputs. Indeed, the tracking performance of the 2D and 3D trajectories are displayed in Figs. 18 and 19. On the other hand, the proposed method generates continuous control signals as displayed in Fig. 20, which reduces chattering and improves the closed-loop system tracking control performance.

6 | CONCLUSIONS

This paper proposed a FO command filtered-based recursive finite-time control using a nonsingular terminal sliding mode technique for high-order uncertain nonlinear systems under disturbances with unknown bounds. The proposed control is developed to get beyond the limitations of existing finite-time tracking controllers like the TSM control. Furthermore, in the proposed approach, the reaching phase is removed, the explosion of complexity in the control problem is avoided, and a chattering alleviation property is achieved. Then, this fractional-order strategy has been applied to control a quadrotor UAV system in different scenarios affected by increasing disturbance amplitudes and frequencies. This technique has been proved to be an appropriate solution for controlling such systems and ensuring the needed tracking. Furthermore, simulation results have demonstrated the effectiveness of the proposal even in comparison with an existing approach in the literature.

7 | BIBLIOGRAPHY

References

1. V. Utkin, (1977) Variable structure systems with sliding modes, IEEE Transactions on Automatic control, vol. 22, no. 2, pp. 212-222.

2. Y. Shtessel, C. Edwards, L. Fridman, and A. Levant (2014) Sliding mode control and observation, ser. Control Engineering. Birkh´auser.

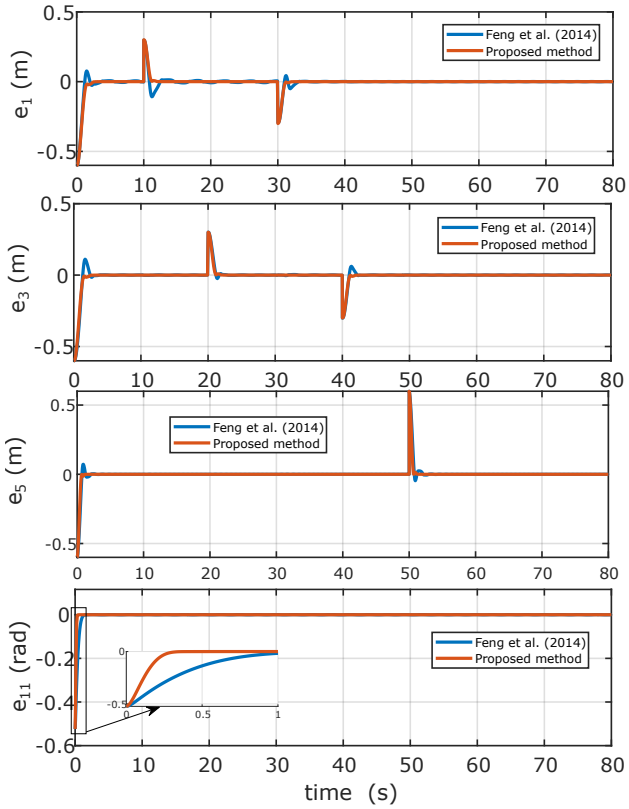

FIGURE 5 Simulation results showing the tracking errors performance of each controller: control in Feng et al. (2014) (—) and proposed method (—) (Nominal model).

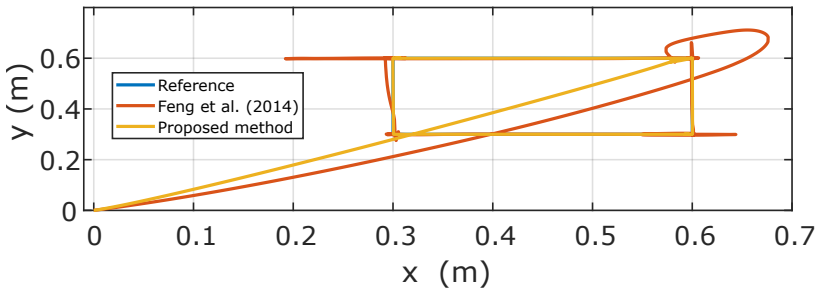

FIGURE 6 Simulation results showing the quadrotor trajectory performance in the 2D environment of each controller: control in Feng et al. (2014) (—) and proposed method (—) (Nominal model).

3. V. Utkin and J. Shi (1996) Integral sliding mode in systems operating under uncertainty conditions,âĂİ in 35th IEEE conference on decision and control, vol. 4. IEEE, pp. 4591-4596.

4. A. Ferrara, G. P. Incremona, and M. Cucuzzella, (2019) Advanced and Optimization Based Sliding Mode Control: Theory and Applications. Philadelphia, PA, USA: Society for Industrial and Applied Mathematics.

5. G. P. Incremona, M. Rubagotti and A. Ferrara, (2017) Sliding Mode Control of Constrained Nonlinear Systems. IEEE Transactions on Automatic Control, vol. 62, no. 6, pp. 2965-2972.

6. G. P. Incremona, L. Mirkin and P. Colaneri, (2022) Integral Sliding-Mode Control With Internal Model: A Separation. IEEE Control Systems Letters, vol. 6, pp. 446-451.

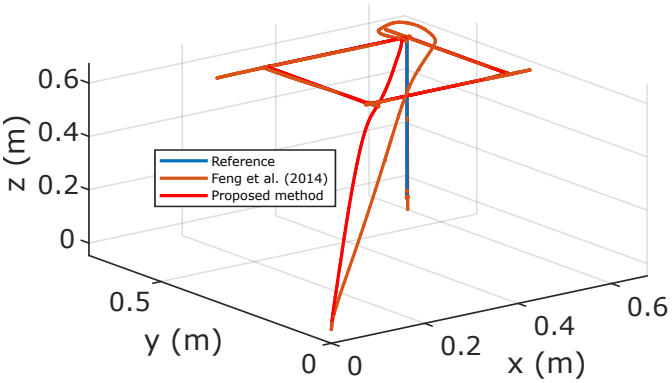

FIGURE 7 Simulation results showing the quadrotor trajectory performance in the 3D environment of each controller: control in Feng et al. (2014) (__) and proposed method (__) (Nominal model).

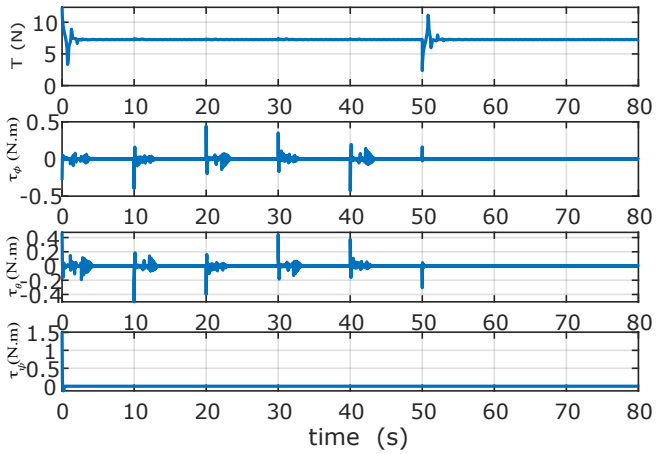

FIGURE 8 Simulation results showing the quadrotor control inputs (Nominal model).

7. Bhat, S. P., Bernstein, D. S. (1997). Finite-time stability of homogeneous systems. In Proc. American control conf (pp. 1073-1078).

8. Yu, X., Feng, Y., and Man, Z. (2020) Terminal Sliding Mode Control - An Overview. IEEE Open J. Ind. Electron. Soc., 2, 36-52.

9. Feng, Y., Yu, X., and Man, Z. (2002) Non-singular terminal sliding mode control of rigid manipulators. Automatica, 38 (12), 2159-2167.

10. Feng, Y., Yu, X., and Han, F. (2013) Automatica On nonsingular terminal sliding-mode control of nonlinear systems. Automatica, 1-8.

11. S. Yu, X. Yu, B. Shirinzadeh, and Z. Man (2005) Continuous finite- time control for robotic manipulators with terminal sliding mode, Automatica, vol. 41, no. 11, pp. 1957-1964, 2005.

12. Feng, Y., Han, F., and Yu, X. (2014) Chattering free full-order sliding-mode control. Automatica, 50 (4), 1310-1314.

13. Utkin, V. (1992). Sliding modes in control and optimization. Berlin, Germany: Springer-Verlag.

14. Bartolini, G., Ferrara, A., and Usai, E. (1998). Chattering avoidance by second-order sliding mode control. IEEE Transactions on Automatic Control, 43(2), 241-246.

15. Levant, A. (1998). Robust exact differentiation via sliding mode technique. Automatica, 34(3), 379-384.

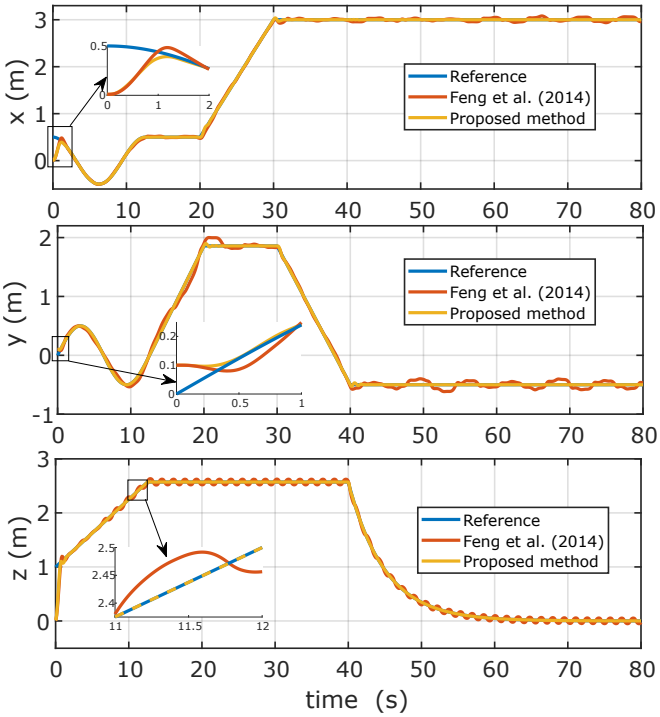

FIGURE 9 Simulation results showing the position performance of each controller;: reference (—), control in Feng et al. (2014) (—), and proposed method (—) (Increasing disturbance amplitudes).

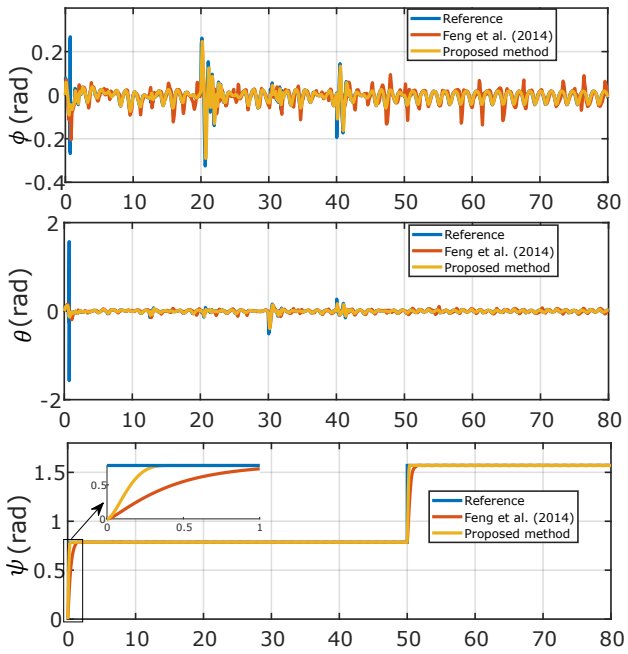

FIGURE 10 Simulation results showing the attitude performance of each controller; reference (—), control in Feng et al. (2014) (—), and proposed method (—) (Increasing disturbance amplitudes).

16. Shtessel, Y. B., Shkolnikov, I. A., and Brown, M. D. J. (2003). An asymptotic second- order smooth sliding mode control. Asian Journal of Control, 5(4), 498-504.

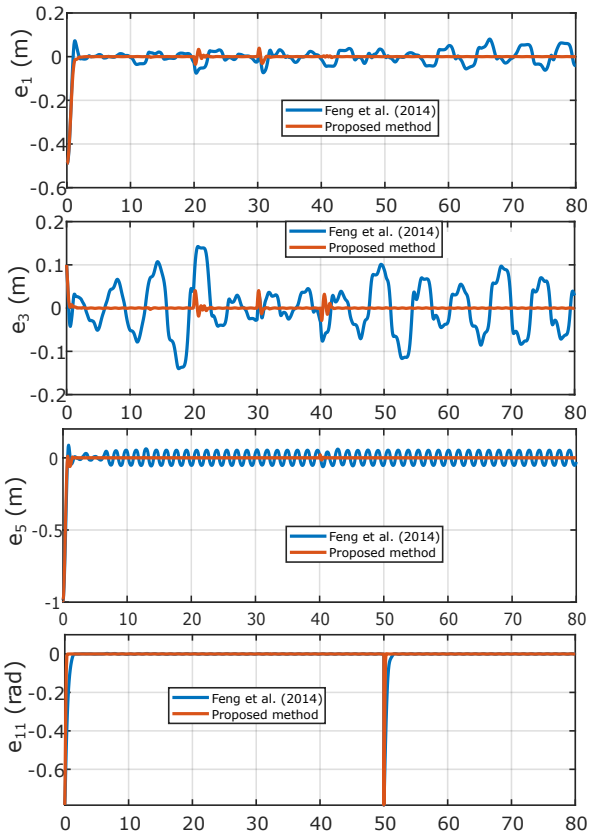

FIGURE 11 Simulation results showing the tracking errors performance of each controller; control in Feng et al. (2014) (—) and proposed method (—) (Increasing disturbance amplitudes).

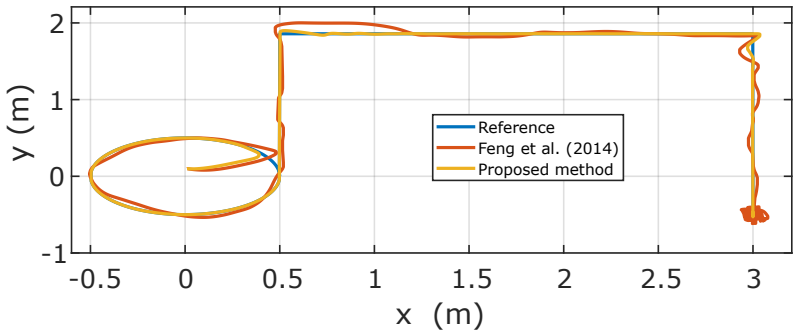

FIGURE 12 Simulation results showing the quadrotor trajectory performance in the 2D environment of each controller; Feng et al. (2014) (—) and Proposed method (—) (Increasing disturbance amplitudes).

17. Shao, K., Zheng, J., Huang, K., Wang, H., Man, Z., and Fu, M. (2020) Finite-Time Control of a Linear Motor Positioner Using Adaptive Recursive Terminal Sliding Mode. IEEE Trans. Ind. Electron., 67 (8), 6659-6668.

18. Song Z, Duan C, Wang J, Wu Q. Chattering-free full-order recursive sliding mode control for finite-time attitude synchronization of rigid spacecraft. J Frankl Inst. 2018;356(2):998-1020.

19. Utkin VI, Poznyak AS. Adaptive sliding mode control with application to super-twist algorithm: equivalent control method. Automatica. 2013;49(1):39-47.

20. Shtessel Y, Taleb M, Plestan F. A novel adaptive-gain supertwisting sliding mode controller: methodology and application. Automatica. 2012;48(5):759-769.

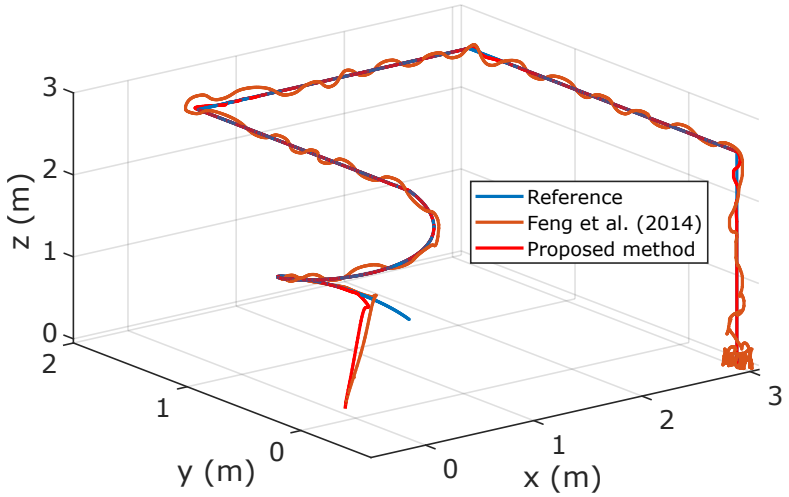

FIGURE 13 Simulation results showing the quadrotor trajectory performance in the 3D environment of each controller; control in Feng et al. (2014) (—) and proposed method (—) (Increasing disturbance amplitudes).

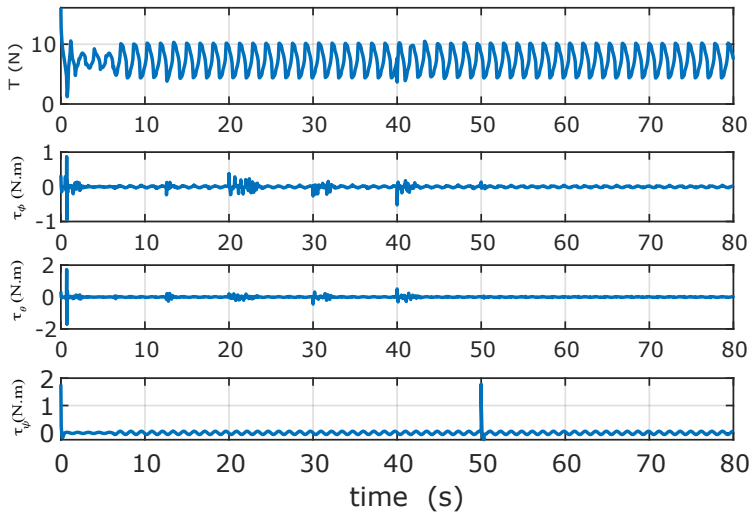

FIGURE 14 Simulation results showing the quadrotor control inputs (Increasing disturbance amplitudes).

21. Plestan F, Taleb M, Bououlid B.. High order integral sliding mode control with gain adaptation. Paper presented at: Proceedings of the 2013 European Control Conference (ECC). Zurich, Switzerland; July 17, 2013:890-895; IEEE.

22. Zhu, Z. Liang, H. Liu, Y. Xue, H (2021) Command filtered event-triggered adaptive control for MIMO stochastic multiple time-delay systems. I. J. of Rob. and Non. Cont., https://doi.org/10.1002/rnc.5868.

23. Han, S. (2020) Fractional-order command filtered backstepping sliding mode control with fractional-order nonlinear disturbance observer for nonlinear systems. J. Franklin Inst., 357 (11), 6760-6776.

24. Song, S., Park, J.H., Zhang, B., Song, X., and Zhang, Z. (2021) Adaptive Command Filtered Neuro-Fuzzy Control Design for Fractional-Order Nonlinear Systems with Unknown Control Directions and Input Quantization. IEEE Trans. Syst. Man, Cybern. Syst., 51 (11), 7238-7249.

25. Ma, J., Park, J.H., and Xu, S. (2021) Command-Filter-Based Finite-Time Adaptive Control for Nonlinear Systems with Quantized Input. IEEE Trans. Automat. Contr., 66 (5), 2339-2344.

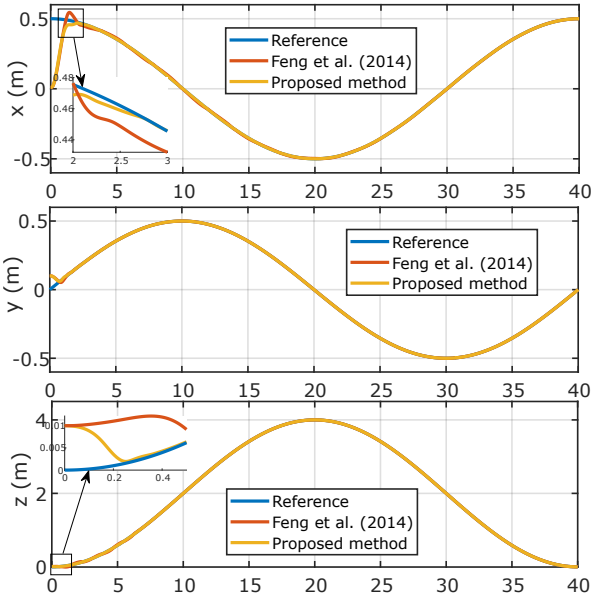

FIGURE 15 Simulation results showing the position performance of each controller: reference (__), control in Feng et al. (2014) (__), and proposed method (__) (Increasing disturbance frequencies).

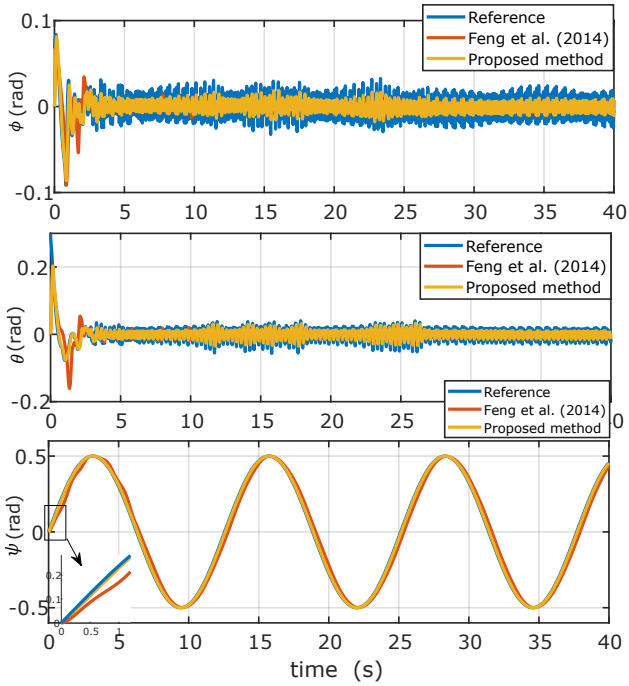

FIGURE 16 Simulation results showing the attitude performance of each controller; Reference (__), Feng et al. (2014) (__), and Proposed method (__) (Increasing disturbance frequencies).

26. Zhang, J., Xia, J., Sun, W., Wang, Z., and Shen, H. (2019) Command filter-based finite-time adaptive fuzzy control for nonlinear systems with uncertain disturbance. J. Franklin Inst., 356 (18), 11270-11284.

27. Zhu, X., Ding, W., and Zhang, T. (2021) Command filter-based adaptive prescribed performance tracking control for uncertain pure-feedback nonlinear systems with full-state time-varying constraints. Int. J. Robust Nonlinear Control, 31 (11), 5312-5329.

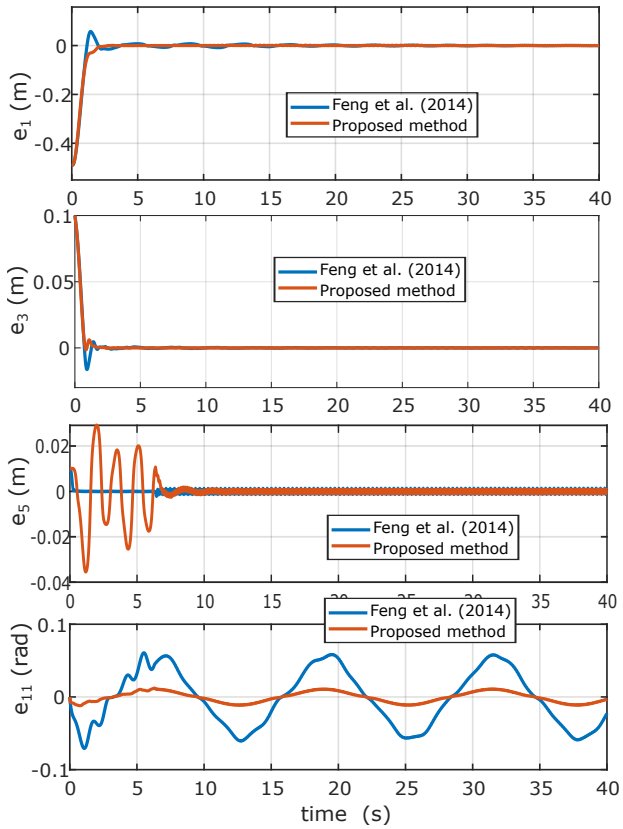

FIGURE 17 Simulation results showing the tracking errors performance of each controller; Feng et al. (2014) (—) and Proposed method (—) (Increasing disturbance frequencies).

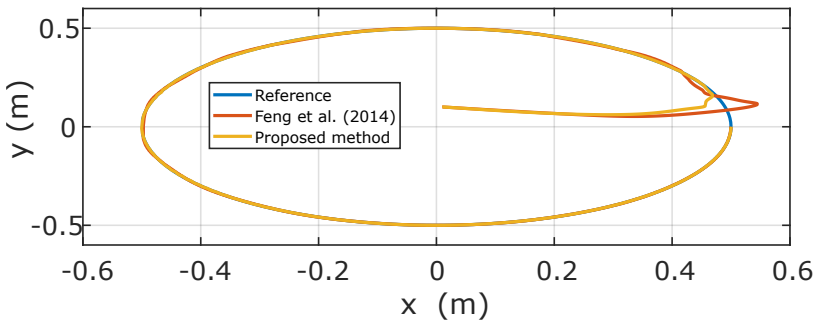

FIGURE 18 Simulation results showing the quadrotor trajectory performance in the 2D environment of each controller: control Feng et al. (2014) (—) and proposed method (—) (Increasing disturbance frequencies).

28. Wei, W., and Zhang, W. (2021) Command-Filter-Based Adaptive Fuzzy Finite-Time Output Feedback Control for State-Constrained Nonlinear Systems With Input Saturation. IEEE Trans. Fuzzy Syst., 6706 (c), 1-1.

29. I. Podlubny, Fractional Differential Equations. New York: Academic, 1999.

30. S. Das, Functional Fractional Calculus for System Identification and Controls. Heidelberg: Springer-Verlag, 2008.

31. I. Podlubny, Geometric and physical interpretation of fractional integration and fractional differentiation, Fractional Calculus & Applied Analysis, vol. 5, pp. 367-386, 2002.

32. Shao K. Nested adaptive integral terminal sliding mode control for high-order uncertain nonlinear systems. Int J Robust Nonlinear Control. 2021;31:6668-6680. https://doi.org/10.1002/rnc.5631.

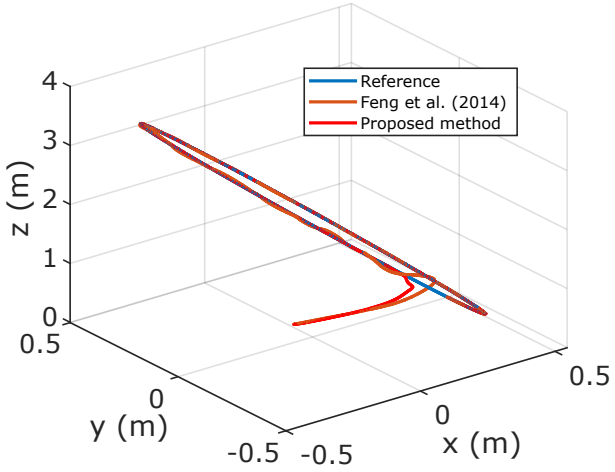

FIGURE 19 Simulation results showing the quadrotor trajectory performance in the 3D environment of each controller: Feng et al. (2014) (__), and proposed method (__) (Increasing disturbance frequencies).

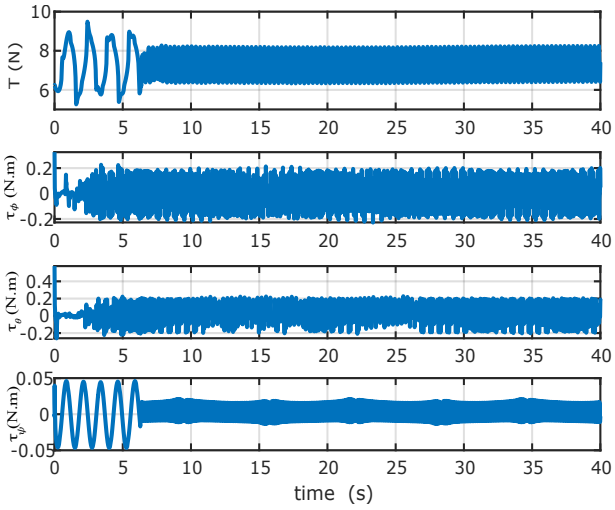

FIGURE 20 Simulation results showing the quadrotor control inputs (Increasing disturbance frequencies).

33. M. Labbadi and M. Cherkaoui, (2018) Robust adaptive nonsingular fast terminal sliding-mode tracking control for an uncertain quadrotor UAV subjected to disturbances, ISA Trans., vol. 99, pp. 290-304, 2019.. 540-544.

How to cite this article: M. Labbadi, and M. Defoort, G. P. Incremona, M. Djemai Fractional-Order, … , …